A conceptual semidistributed model of the Coulazou River as a tool for assessing surface water-karst groundwater interactions during flood in Mediterranean ephemeral rivers

V. Bailly-Comte, V. Borrell-Estupina, H. Jourde, Séverin Pistre

A conceptual semidistributed model of the Coulazou River as a tool for assessing surface water–karst groundwater interactions during flood in Mediterranean ephemeral rivers

V. Bailly-Comte,[1,2] V. Borrell-Estupina,[1] H. Jourde,[1] and S. Pistre[1]

Received 1 October 2010; revised 12 July 2012; accepted 31 July 2012; published 21 September 2012.

[1] This study aims to assess surface water–karst groundwater interactions during floods in the Mediterranean karst watershed of the Coulazou River (southern France) using a conceptual semidistributed model at 5 min time steps. The kinematic wave routing approximation is used for the transfer of surface flow, while overflows from a linear underground reservoir account for karst flows along the riverbed. After calibration, values of parameters and simulated time series are compared to independent physical measurements. Results show that direct runoff can be neglected on the karst terrains. In addition, this study demonstrates that, in some cases, karst watersheds can be considered as relatively poor systems of regulation but strong systems of amplification or generation of floods and flash floods, depending on rainfall characteristics and also on groundwater level conditions prior to the flood event. Considering that the flood peak is the most important factor defining flash flood hazard, it is shown that the flood hazard regulation effect of the karst is relatively limited for low water table conditions prior to the flood, while the aggravating effect for high water table conditions may be higher than 80% with respect to expected values from surface runoff only. These results show that understanding groundwater–surface water interactions is crucial for describing the flash flood dynamics in karst terrains.

Citation: Bailly-Comte, V., V. Borrell-Estupina, H. Jourde, and S. Pistre (2012), A conceptual semidistributed model of the Coulazou River as a tool for assessing surface water–karst groundwater interactions during flood in Mediterranean ephemeral rivers, *Water Resour. Res.*, *48*, W09534, doi:10.1029/2010WR010072.

1. Introduction and Background

[2] Flood hazards related to flash floods constitute an important field of research within the hydrologic community due to their large socioeconomic and environmental impacts [e.g., *Llasat et al.*, 2010]. Consequently, great attention has been devoted to flash floods since the mid-1990s, leading to a better understanding of the hydrologic mechanisms by which flash floods are generated. Although various definitions of flash floods have been proposed in different contexts, we will use the following definition in this work: a sudden but short-duration hydrologic response in a river, whatever the space and time structure of the rainy event, and whatever the overland flow generated process. Accordingly, flash floods are rapidly developing floods with little warning, which constitutes the main challenge for flash flood hazard management.

[3] Numerous research projects have led to substantial improvement in flash flood warning, especially in Europe (see, for example, the Achieving Technological Innovation in Flood Forecasting (ACTIF) research project (http://www.actif-ec.net/) or FLASH (http://flash-eu.tau.ac.il/index.php): Observations, Analysis and Modeling of Lightning Activity in Thunderstorms, for use in Short-Term Forecasting of Flash Floods), with a major focus on the Mediterranean region which unfortunately experienced several catastrophic flash floods in the last few decades [*Bonacci et al.*, 2006; *Delrieu et al.*, 2005; *Gaume et al.*, 2009; *Gaume and Bouvier*, 2004; *Gaume et al.*, 2004; *Huet et al.*, 2003; *López-Chicano et al.*, 2002; *Mijatovic*, 1988]. While the influence of antecedent precipitation/soil moisture on flash flooding is typically considered important, groundwater (GW) contribution to surface flows is assumed to be negligible, due to its longer response time [*Borga et al.*, 2007; *Doswell*, 1994; *Doswell et al.*, 1996; *Norbiato et al.*, 2008, 2009].

[4] In recent times, another type of flash flooding has been described in karst terrains [*Bailly-Comte et al.*, 2009, 2008b; *Bonacci et al.*, 2006; *De Waele et al.*, 2010; *Jourde et al.*, 2007; *López-Chicano et al.*, 2002; *Mijatovic*, 1988], despite their highly permeable infiltration zone, which highlights that GW surge flows may also have a great influence on flash flood genesis and transfer in karst area. This is of particular importance since karst aquifers widely outcrop in the Mediterranean basin [*Bakalowicz*, 2005], and most surface streams interact with them, providing a unique source of base flow for perennial streams during the dry

[1]Hydrosciences Laboratory, UMR 5569, University of Montpellier 2, Montpellier, France.
[2]Now at BRGM, Water Department, Montpellier, France.

Corresponding author: V. Bailly-Comte, BRGM–D3E/NRE, Water Department, 1039 rue de Pinville, 34000 Montpellier, France. (v.baillycomte@brgm.fr)

0043-1397/12/2010WR010072

season [e.g., *Hazan and Lazarevitch*, 1967] but also modifying the short-term hydrologic response of the stream. Karst aquifers have complex and unusual hydrodynamics due to the high heterogeneity of voids created and organized by groundwater flow over hydrogeological history (karstification processes). As a result, karst flash floods show unusual characteristics influenced by specific structures of storage and drainage in karst systems, inducing unique hydrodynamics. During floods, these characteristics clearly appear at the surface where karst features like poljes, sinkholes or temporary springs drive the interactions between surface water (SW) and GW [*Bailly-Comte et al.*, 2009; *Bonacci et al.*, 2006]. In addition, karst groundwater drainage rarely coincides with surface drainage patterns.

[5] Hydrodynamic interactions between SW and GW have been successfully described in karst watersheds according to the type of hydraulic connection and the direction of flows between the river reaches and the phreatic zone of the aquifer [*Bailly-Comte et al.*, 2009]. First, *perched* streams, as opposed to *connected* streams, are hydraulically disconnected from the phreatic zone of the aquifer, which means that there is a vadose zone below the riverbed. Second, *losing* streams, as opposed to *gaining* streams, lose water by outflow through the riverbed. River reaches often gain or lose water at different places and/or different times during the flood event and are thus described as *losing/gaining* reaches with a possible predominant gaining or losing direction of flow. An additional case has been identified after intense rainfall occurring in low GW conditions when karst conduits under great pressure simultaneously recharge the carbonate matrix of the aquifer (losing stream) and the river (gaining stream) [*Bailly-Comte et al.*, 2009]. This basic description of SW–karst GW interactions has been performed using quantitative (water level) and qualitative (temperature and specific electrical conductivity) measurements during floods in both SW and groundwater.

[6] The use of hydrologic models that are nonspecific to karst watersheds give poor results [*Virginia Department of Conservation and Recreation*, 2006], even for calibration of flash flood warning models [*Norbiato et al.*, 2008]. For instance, *Jourde et al.* [2007] used a physically based hydrologic model at a 5 min time step integrating a digital elevation model to highlight the inability of a standard rainfall-runoff model to simulate flood hydrographs at the exit of a karst watershed. Besides, knowledge about the spatial distribution of voids, hydraulic conductivities and storage coefficient within karst aquifers is often insufficient for the needs of a fully physically based model of karst hydrodynamics. For this reason, many authors have used simple daily rainfall/discharge conceptual models to reproduce karst spring hydrographs by a series of linear or nonlinear reservoirs accounting for different components of storage and transfer within karst aquifers [*Arikan*, 1988; *Barrett and Charbeneau*, 1997; *Fleury et al.*, 2007; *Jukić and Denić-Jukić*, 2009; *Le Moine et al.*, 2008; *Padilla and Pulido-Bosch*, 2008; *Rimmer and Salingar*, 2006]. Another type of rainfall/discharge model based on the convolution integral involves one or more transfer functions to describe various storage and flow processes that occur in a karst aquifer: transfer functions are usually derived from the analysis of time series using inverse modeling methods without application of physical laws. They can be used to infer the functioning of karst aquifers [*Bailly-Comte et al.*, 2008b, 2008c; *Bouchaou et al.*, 2002; *Dreiss*, 1983; *Larocque et al.*, 1998; *Mangin*, 1984; *Padilla and Pulido-Bosch*, 1995; *Panagopoulos and Lambrakis*, 2006; *Rahnemaei et al.*, 2005] or directly as a black-box model of the whole or a part of the karst system [*Dörfliger et al.*, 2009; *Jukić and Denić-Jukić*, 2004, 2006; *Labat et al.*, 1999, 2000a, 2000b; *Long*, 2009; *Long and Derickson*, 1999; *Maréchal et al.*, 2008]. Black-box models have also been used within a reservoir model to define transfer functions of each reservoir [*Jukić and Denić-Jukić*, 2009; *Padilla and Pulido-Bosch*, 2008]. Among these studies, *Labat et al.* [1999] used high-frequency data (30 min) to construct linear and nonlinear kernel functions of rainfall/discharge relationships in karstic spring.

[7] As a result, all these previous modeling works mainly focused on karst spring hydrographs, and most often at a daily time step. To our knowledge, there is no example of modeling study of floods in a karstic river that explicitly accounts for GW-SW hydrodynamic interactions at a time scale that is consistent with flash flood duration observed in Mediterranean ephemeral streams, typically much shorter than a day [*Camarasa Belmonte and Segura Beltran*, 2001]. In this context, our study aims to develop a conceptual semidistributed model of flood genesis and propagation in a karst watershed at short time step (5 min) accounting for processes specific to karst hydrology. We investigate the role of a karst aquifer on the genesis and transfer of flash floods using eight flood events of minor to extreme intensities in the Coulazou River, a typical ephemeral Mediterranean river. The experimental karst watershed of this river is used to discuss the physical meaning of each model parameter by comparing results of the calibration procedure with independent physical measurements within the aquifer. This modeling approach is performed with two objectives: (1) exploring concepts of karst flash flooding and (2) providing a quantitative estimate of the influence of karst on the genesis and propagation of floods in an ephemeral stream.

2. Case Study and Model Structure

2.1. Hydrogeological Settings and Monitoring Network

2.1.1. Climatic, Hydrological and Geological Settings

[8] The studied area is located 20 km west from Montpellier, southern France (Figure 1). The Coulazou River is a typical Mediterranean ephemeral river that exhibits a dry streambed only few days after rainfall events. In this Mediterranean basin, rainfall events of strong intensities are usually observed in late summer or fall, especially on the upstream part of the watershed of the Coulazou River (Figure 1). For instance, intensities close to 180 mm/h were recorded in September 2005 on this 21 km^2 upstream watershed defined by Q_1 (Figure 1). Such torrential rainfall results in flash flooding caused by direct runoff on relatively impervious marly Eocene limestone covered by Oligocene clastic sedimentary rocks to the north. These floods are characterized by narrow flood peaks with short time lags (less than a day) as they reach karst terrains to the south (three examples are shown in Figure 5, left); these allogenic surface flows drive the allogenic recharge of the karst aquifer.

[9] Karst terrains are composed of a highly folded, fractured and karstified sedimentary sequence of lower Jurassic to upper Jurassic age limestone that widely outcrops and forms the calcareous plateau of the Aumelas Causse

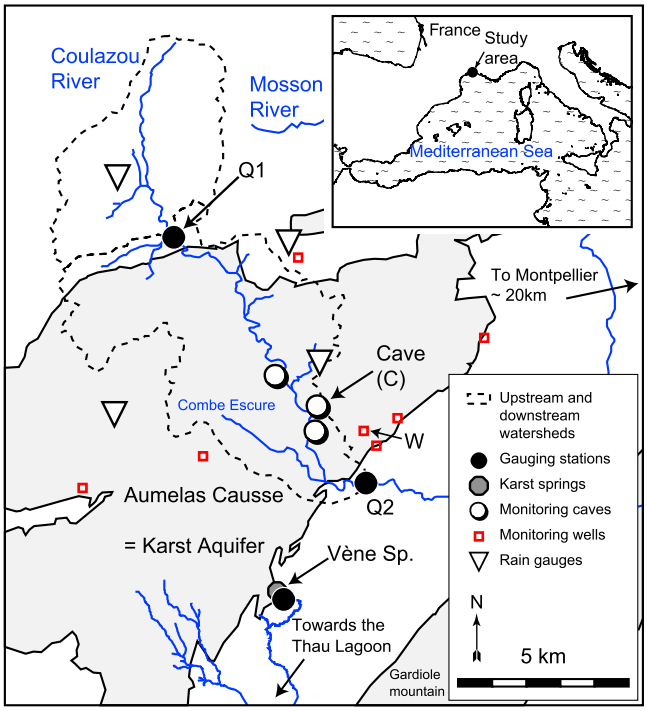

Figure 1. Study area and monitoring network with some hydrologic and hydrogeologic information.

(Figure 1). Soils are rare, but epikarst features and endoreic areas are common, so that direct surface runoff is not significant. Some Oligocene clastic sedimentary rocks also outcrop on the Aumelas Causse in the thalweg of the Combe Escure intermittent stream, i.e., within the shaded zone labeled as karst aquifer in Figure 1. These nonkarst and relatively impervious formations suggest that the Combe Escure stream may also contribute to surface flows in the Coulazou River (Figure 1). The studied karst system is known as the Aumelas-Thau karst system, since groundwater is partly drained southwestward below a tertiary detritic basin toward the Thau lagoon [*Bonnet and Paloc*, 1969]. This regional-scale flow system does not have a major influence on the dynamics of flash flood generation in the Coulazou basin. As a result, a karst/river system limited to the south by the Vène Spring has been defined [*Bailly-Comte et al.*, 2009], including more than 15 karst features temporary acting as springs or sinkholes along the 10 km long riverbed [*Bourrier*, 2001].

2.1.2. Monitoring Network

[10] A monitoring network covering the karst aquifer and including surface runoff measurements was constructed in the region to assess karst/river hydrodynamic interactions (Figure 1). Rainfall is measured using 4 rain gauges distributed over the 61 km^2 Coulazou watershed at a 5 min interval using a 0.2 mm tipping bucket. Discharge in the river is measured using gauging stations upstream and downstream from the karst aquifer at a 5 min interval (Q_1 and Q_2, Figure 1). River stage in Q_1 is converted to runoff based on a rating curve using flow velocity measurements and the Manning's equation for higher water levels. For Q_2, stage is converted to discharge based on flow velocity measurements above a weir crest and a steady gradually varied flow model in 1D using HEC-RAS [*Bailly-Comte*, 2008; *U.S. Army Corps of Engineers* (*USACE*), 2002b]. Q_1 and Q_2 are the names given to the gaging station where the Q_1 and Q_2 discharge time series are recorded for the upstream watershed and the whole watershed shown in Figure 1, respectively.

[11] Water level, and eventually temperature and specific electrical conductivity (SpC) have been measured in 7 wells and 3 caves since 2004. As part of this network, C (Figure 1) is the main cave in the riverbed and is called Puits de l'aven. It is at least 1300 m long with perennial water in its base [*Douchet*, 2007]. During floods it acts as a spring and/or a sinkhole along the riverbed and thus is formally an estavelle. W (Figure 1) is a 120 m deep, uncased well which has been drilled into the Jurassic limestone. Previous studies showed that water level in W gives a measure of the water level in the fractured carbonate matrix influenced by the Coulazou River [*Bailly-Comte et al.*, 2009, 2008c].

2.1.3. Hydrodynamics of the Aumelas-Thau Karst System at the Flood Event Scale

2.1.3.1. Activation of an Upper Karst Drainage Network in Flood Conditions

[12] During floods, karst overflows first occur in the downstream part of the river and propagate to the upstream part as GW level increases [*Jourde et al.*, 2007]. Sinkholes in the riverbed are known to be connected to an upper karst drainage system which formed when the Coulazou River constituted the base level of the karst aquifer. This upper karst drainage system develops horizontally in the vicinity of the river at an altitude close to 47 m above sea level (masl), with numerous water traps; it is normally a vadose portion of the aquifer that conveys infiltrated water to the perennial outlets of the Aumelas-Thau karst system, or to the Vène temporary spring in high water table condition, but it can temporarily act as phreatic conduits during a flood, conveying GW to the river through sinkholes back flooding [*Bailly-Comte et al.*, 2010]. In this later case, the upper karst drainage network is said to be activated. For instance, Figure 2 illustrates how the aquifer responds to the activation of the upper karst drainage network during floods: The water level evolution in W denotes rapid pressure transfer in high water conditions through a well-developed conduit system, which is the upper karst drainage network, exemplified by the fast water level evolution in C. However, this upper karst drainage network is disconnected when the water level in W falls below approximately 47 masl, inducing a higher influence of matrix flows [*Bailly-Comte et al.*, 2010]. Thus, 47–48 masl is considered as the groundwater level condition in W for the activation of the upper karst drainage network (Figure 2). More precisely, in high water table conditions, this upper karst drainage system drains GW outside from the Coulazou watershed until the maximum discharge capacity [*Bonacci*, 2001] of the Vène spring is reached. The maximum discharge capacity is not the maximum discharge that can be observed at the spring, but the discharge threshold at the spring above which the relationship between the hydraulic head in the conduit system and the spring discharge is modified. This occurs when the karst drainage network connected to the spring is submerged, which induces an increase of the pressure head in the conduit network that led to the activation of the upper karst drainage network in the riverbed (i.e., cave C in February 2006 on Figure 2). This discharge capacity has been estimated at

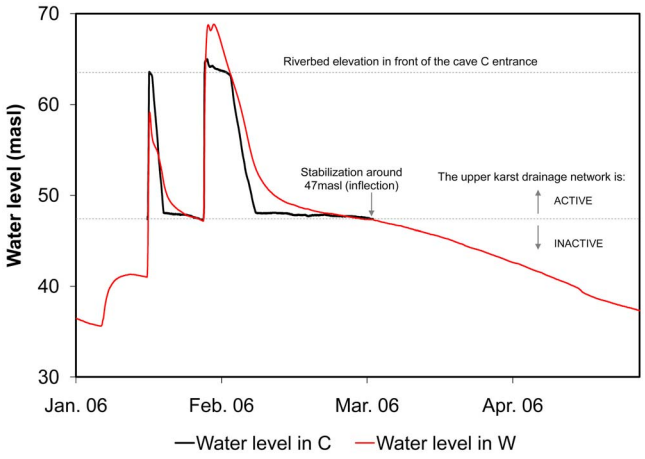

Figure 2. Water level evolution in a sinkhole (C) and in a well (W) during high water table conditions showing the activation of an upper karst drainage network.

5.5 m^3/s using the hourly discharge distribution function (or flow duration curve) at the spring between 2002 and 2007 [*Bailly-Comte et al.*, 2009].

[13] The water level in W (Figure 1) prior to each flood event is denoted h_W. At this site, *Bailly-Comte et al.* [2008c] showed that h_W can be used to describe the initial state of the aquifer. Furthermore, *Bailly-Comte et al.* [2009] found that SW and GW bodies are likely to be connected during flood events if h_W is higher than 35 masl. Temperature and SpC time series in the cave C also give information about the direction of flow between the aquifer and the river during the flood transfer. These measurements are used to identify when the river is losing or gaining water. Accordingly, *Bailly-Comte et al.* [2009] showed that the river is fed by the aquifer (acting as gaining stream) if h_W is close to 47 masl, which means that the upper karst drainage system was already active prior to the recharge event (Figure 2).

2.1.3.2. Flood Dynamics

[14] Eight flood hydrographs (Table 1) are used for assessment of the influence of karst on flood genesis and propagation in this ephemeral Mediterranean river. This monitoring site is part of the MEDYCYSS observatory dedicated to hydrodynamics and flood events at different scales in Mediterranean karst basins; the data set used for model calibration and hydrodynamic interpretations may be requested through the MEDYCYSS Web site (http://www.medycyss.org). Characteristics of GW-SW interactions are given in Table 1. Each event is classified according to flow direction between GW and SW and the type of hydraulic connection, as discussed above.

[15] All flood events are characterized by short time to rise (duration of the rising limb), less than a day and often less than an hour. In addition, floods are short (less than a day) when the river is not gaining water but can last more than 8 days (210 h) when GW significantly contributes to surface flows, which is discussed in section 2.2. These observations allow us to define these events as flash floods following our definition based both on short flood duration and short response time (time to rise in Table 1).

2.1.3.3. Flow Coefficient and Peak Specific Discharge Analysis

[16] The peak specific discharge clearly decreases between Q_1 and Q_2 if the river is losing water from upstream to downstream, i.e., when the river crosses the karst aquifer, but it remains relatively high (e.g., 0.9 $m^3/s/km^2$ in September 2005), or even slightly increases (e.g., 0.3 to 0.4 $m^3/s/km^2$ in April 2004) if the river is gaining water from the karst aquifer.

[17] The flow coefficient is the portion of rainfall that is converted to surface flow at the outlet of a topographic catchment area. According to *Norbiato et al.* [2009], we expect higher values at the outlet Q_1 of the upstream basin characterized by relatively impermeable terrains than at the outlet Q_2 because of the higher permeability of karst terrains in the downstream part. Flow coefficients are extremely variable on this site, and, like the maximum specific discharge, the evolution of the flow coefficient between Q_1 and Q_2 is directly related to the flow direction between GW and SW, and it thus can be much higher in Q_2. This can be better understood using the ratio of the cumulative rainfall over the

Table 1. Some Characteristics of the Eight Floods Events Recorded in the Coulazou River and the Corresponding River Classification

Date	h_W[a] (masl)	River Classification		Rainfall Up/Down[b]	Peak Specific Discharge ($m^3/s/km^2$)		Flow Coefficient (%)		Time to Rise[d] (h)	Flood Duration[e] (h)
		Flow Direction	Hydraulic Connection		Q_1	Q_2	Q_1/Q_2	Apparent[c]		
6 Oct 2004	31	Losing	Perched	122/28	1.2	0.3	8/3	−7	0.5	10
18 Oct 2006	46	Losing	Connected	nd/11	0.4	0.1	nd	nd	0.5	19
6 Sep 2005	24	Losing/ Gaining	Perched	257/154	1.9	0.9	11/11	12	0.75	<10[f]
12 Nov 2005	42	Losing/ Gaining	Connected	60/53	0.1	0.1	16/14	13	2.5	98
24 Sep 2006	35	Losing/ Gaining	Connected	68/62	0.1	0.1	6/5	5	1.6	38
15 Jan 2006	41	Losing/ Gaining	Connected	44/46	0.1	0.2	21/17	15	3.25	106
28 Apr 2004	49	Gaining	Connected	110/69	0.3	0.4	12/26	39	6.25	100
27 Jan 2006	47	Gaining	Connected	208/200	0.9	0.9	24/72	100	14	210

[a]Water level in W prior to the flood.
[b]Cumulated rainfall estimated on the upstream and downstream part of the catchment (Figure 1); nd, not discernible.
[c]Apparent flow coefficient is defined in the text.
[d]The time to rise refers to the duration of the rising limb recorded in Q_2; the flood in this ephemeral river arbitrary starts when $Q_2 > 1$ m^3/s.
[e]Flood duration refers to the duration of the flood recorded in Q_2 that arbitrary starts when $Q_2 > 1$ m^3/s and ends when $Q_2 < 0.1$ m^3/s. It is thus the base time of the flood event, with eventually an additional base flow period when it exists.
[f]Another flood event prevents from precisely estimating the flood duration, which would have been probably less than 10 h.

karst terrains delimited by topographic boundaries to the gain of water in the river as it flows over the karst terrains; this ratio is denoted *apparent flow coefficient* in Table 1 and is computed as follows:

$$\left(\int_T Q_2(t).dt - \int_T Q_1(t).dt\right) / \left(R \times S_{topo}\right) \quad (1)$$

where $Q_i(t)$ [L^3T^{-1}] is the discharge time series recorded at the station Q_i (i = 1,2, Figure 1), S_{topo} [L^2] is the karst portion of the catchment area that is drained toward the Coulazou River between Q_1 and Q_2 according to topographic boundaries. S_{topo} equals the downstream part of the watershed in Figure 1 (34 km^2), and R [L] is the cumulative rainfall that gives rise to the flood. It is estimated over the surface S_{topo} using the 3 downstream rain gauges (see Figure 1) in proportion to the area each rain gauge is assumed to represent (Thiessen polygon method). T [T] is the duration of streamflow in the ephemeral river in response to the rainfall event. The flood arbitrarily ends when $Q_2 <$ 0.1 m^3/s.

[18] Results show that the apparent flow coefficient may be negative when the river is predominantly losing water, which means that the river loses more water than it gains on the karst subcatchment. The apparent flow coefficient may also reach extremely high values (even close to 100%). Considering the inherent water storage in the soil or in the vadose zone, as well as the recharge of the aquifer, such high values are consistent with neither surface hydrology nor groundwater processes over a natural ground cover, indicating that the recharge area over the karst terrains is larger than the topographic watershed shown in Figure 1.

[19] Both maximum specific discharge and flow coefficients show that the karst aquifer strongly modifies the flood transfer; it either attenuates or amplifies it in term of both intensity and volume depending on hydrogeological conditions given by h_W (Table 1). More details about hydrodynamics of this site may be found in earlier publications [*Bailly-Comte et al.*, 2009, 2008b, 2008c, 2010; *Jourde et al.*, 2007]. All these results constitute the rationale for the model structure that is described in section 2.2.

2.2. Conceptual Semidistributed Model of a Karst Watershed

2.2.1. Hydrologic Model

2.2.1.1. Excess Precipitation

[20] The watershed of the Coulazou River is split into 3 homogeneous subbasins (Figure 3) for which the rainfall $p(t)$ [L] is considered as spatially uniform at a time step Δt = 5 min. For each subbasin, basic concepts and governing equations for the runoff generation at the event scale is based on the parsimonious *initial and constant loss* model of HEC-HMS [*USACE*, 2002a]: An initial loss, *Ia* [L], is used as an initial condition to represent interception, depression storage and soil moisture deficit. It is assumed that the time duration of a flood in an ephemeral river is short enough to neglect evaporation processes. *Ia* represents the maximum precipitation depth that can fall without runoff. The maximum potential rate of precipitation loss, *fc* [L/T], is assumed to be constant throughout each event. It determines the rate of infiltration that occurs when the initial loss threshold is reached. The excess precipitation $pe(t)$ [L] is computed using

$$pe(t) = \begin{cases} 0 & if \quad P(t) < Ia \\ \max(0, P(t) - Ia - fc \times \Delta t) & if \quad 0 < P(t) - Ia < p(t) \\ \max(0, p(t) - fc \times \Delta t) & if \quad P(t) - Ia > p(t) \end{cases} \quad (2)$$

according to the accumulated precipitation depth since the beginning of the rainfall $P(t)$ [L]. A percentage of impervious area is also specified. On these areas, the excess precipitation equals the precipitation.

[21] The subbasin 1 stands for the upstream watershed defined by Q_1 (Figure 1), where runoff gives rise to allogenic streams. Precipitation is estimated using the rain gauge located in the upstream watershed (Figure 1). Direct runoff observed along the road close to the gauging station is considered with a percentage of impervious area set to 2%, which has been determined during calibration.

[22] The subbasin 2 represents the karst portion of the watershed defined by Q_2 (Figure 1). The precipitation is computed using a weighted average of the 3 other rain gauges with the Thiessen polygon method. These rain gauges cover the recharge area of both the karst aquifer and the watershed of the Coulazou River (Figure 1). Field observations on karst terrains show that the contribution of direct runoff to surface flows in the river can be neglected, even during extreme rainfall events. This particular behavior is considered by setting an unrealistic value of *fc* in equation (2) so that all the rainfall is lost, except on some impervious area. The percentage of impervious area is fixed to 1% during calibration to account for runoff on a few small roads and inhabited areas close to the outlet which can contribute to river flows during intense rainfall events, which is a reasonable calibration result according to the land cover given by the topographic map (Scan25®© IGN2000). It could be set to zero without any consequence on the flood hydrograph simulation if we only focus on the main flood peak and its recession. The resulting precipitation loss is used in section 2.2.2 to compute the diffuse recharge over the karst area (cf. equation (11)).

[23] The subbasin 3 stands for the nonkarst terrains that outcrop on the Aumelas Causse, and where the Combe-Escure intermittent stream (Figure 1) may contribute to surface flows in the Coulazou River. This runoff is most of the time negligible but explains smaller flood peaks prior to the main flood peak. This contribution is thus not considered as karst flow in the model. A percentage of impervious soil has been set to 5% during calibration, accounting for the contribution of Oligocene impermeable terrains that cover the karst aquifer.

2.2.1.2. Subbasin Geometry

[24] Geometry of each subbasin is characterized by two identical rectangular planes with an equivalent length, so that both perimeter and area of the two rectangles equal those derived from topographic boundaries. This equivalent length and the area are given in Table S1 in the auxiliary material.[1] A main channel conveys flows which enter from the two overland flow planes, and eventually from intermediate

[1] Auxiliary materials are available in the HTML. doi:10.1029/2010WR010072.

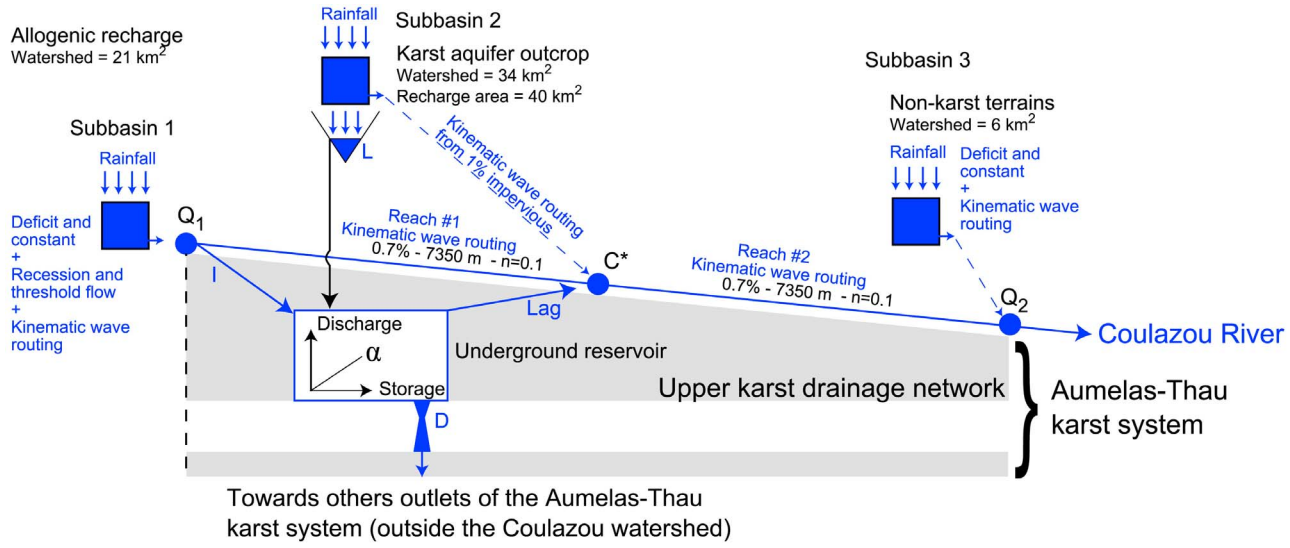

Figure 3. Structure of the conceptual semidistributed model using HEC-HMS.

collectors if tributaries are considered. For the subbasins 1 and 2, outflow from each plane enters a collector that represents the secondary streams. No collectors are specified for the subbasin 3 since no tributaries are connected to the Combe-Escure intermittent stream (Figure 1). The length of the channels and the collectors given in Table S2 are estimated using the topographic map (Scan25®© IGN2000).

2.2.1.3. Main Channel Geometry

[25] Outflows from each subbasin are connected to the main channel standing for the Coulazou River, as shown on Figure 3. More precisely, two identical river reaches account for surface flow routing in the Coulazou River on the karst terrains (River reaches 1 and 2, Figure 3), and each subbasin is connected to the main channel at their appropriate positions (compare Figure 1 with Figure 3). The river has been split into 2 reaches for modeling convenience, since GW contribution to surface flow is also affected by surface flow transfer before reaching Q_2 (Figure 1).

2.2.1.4. Surface Flow Transfer and Governing Equation

[26] Surface flow transfer is based on the kinematic wave approximation for the collectors, the planes of each subbasin and the river reaches 1 and 2, which is solved using a finite difference scheme. The friction slope S_f is approximated by the average bottom slope of the main channel, the collectors and the planes, respectively. Average slopes, length of channels and cross sections are estimated using a topographic map (Scan25®© IGN2000) and field observations. S_f is related to the direct surface runoff Q_{Surf} [L^3T^{-1}] using Manning's equation, which can be written as

$$Q_{Surf} = \frac{A.R_h^{2/3}.\sqrt{S_f}}{n} \quad (3)$$

where A is the rectangular flow section [L^2], R_h is the hydraulic radius [L] and n is the Manning's coefficient [$TL^{-1/3}$]. Manning coefficients vary from 0.04 and 0.06 on the nonkarst terrains to 0.1 on the karst terrains, including the riverbed. Such high values characterize the high roughness of large blocks in the main channel or the highly vegetated floodplain and thalwegs on the planes [*Jourde et al.*, 2007]. Geometrical characteristics and parameters used for each subbasin and river reach are given in Table S1.

2.2.1.5. Base Flow

[27] The base flow recession method of HEC-HMS is used in the subbasin 1 to account for the slow subsurface drainage of soils and river banks in the Oligocene terrains. Flow recession Q_{Recess} [L^3T^{-1}] is computed at time t greater than t_0 using

$$Q_{Recess}(t, t_0, Q_0) = Q_0 \times k^{(t-t_0)} \quad (4)$$

where t_0 is the time after the flood peak when Q_{Surf} defined by equation (3) reaches a specified threshold flow Q_0 [L^3T^{-1}], and k is an exponential decay constant; k is defined as the ratio of the base flow at time t to the base flow 1 day earlier, which implies $k < 1$ and Q_{Recess} becomes 0 at large times. Q_{Base} [L^3T^{-1}] is the base flow that is added to the direct surface runoff. It is computed as the difference between Q_{Recess} and Q_{Surf}:

$$Q_{Base}(t) = Q_{Recess}(t, t_0, Q_0) - Q_{Surf}(t) \quad (5)$$

For complex flood events, i.e., if there is a time t_1 greater than t_0 at which another increase of Q_{Surf} occurs, the base flow becomes

$$Q_{Base}(t) = Q_{Recess}(t, t_1, Q_{Base}(t_1)) \quad (6)$$

In this latter case, if Q_{Surf} exceeds Q_0 another time, then, for time higher than t_2 where t_2 is the time after the second flood peak when Q_{Surf} reaches Q_0, the base flow becomes

$$Q_{Base}(t) = Q_{Recess}(t, t_2, Q_0) - Q_{Surf}(t) + Q_{Recess}(t, t_1, Q_{Base}(t_1)) \quad (7)$$

The procedure given by equations (6) and (7) is repeated if there is another increase of Q_{Surf} before the end of the flood event. Q_0 and k are thus the two parameters of the recession method. The simulated outflow Q_1 [L^3T^{-1}] for the subbasin 1 becomes

$$Q_1(t) = Q_{Base}(t) + Q_{Surf}(t) \quad (8)$$

2.2.2. Underground Reservoir Model

2.2.2.1. Allogenic Recharge

[28] Allogenic recharge Q_{All} [L^3T^{-1}] is considered in the model assuming that the stream sinks at the nonkarst/karst boundary, which is just downstream of Q_1 (Figure 1). The recharge rate depends on the infiltration rate I [L^3/T] of the riverbed, which is driven by the hydraulic gradient between SW and GW. I is assumed to be constant for each flood event, but is expected to reach a maximum value in the case of a perched river. This latter value determines the infiltration capacity of the set of sinkholes along the river. Accordingly, the allogenic recharge is computed for each event as follows, where Q_1 denotes the measured discharge at the gauging station Q_1 (Figure 1):

$$Q_{All}(t) = \min(Q_1(t), I) \tag{9}$$

The resulting surface flow Q_{in} [L^3T^{-1}] that enters the river reach 1 (Figure 3) becomes

$$Q_{in}(t) = Q_1(t) - Q_{All}(t) \tag{10}$$

2.2.2.2. Diffuse Recharge

[29] Diffuse recharge Q_{Diff} [L^3T^{-1}] is estimated using the precipitation loss from subbasin 2 by subtracting initial losses L [L], assuming a recharge area S of 40 km^2 based on estimation of groundwater divides. The L parameter accounts for storage in lower permeability volumes in the epikarst and the vadose zone, the slow drainage from these lower permeability volumes being neglected at the time scale of a flood in an ephemeral stream. The diffuse recharge is computed as follows, with p_L [L] the instantaneous precipitation loss of the subbasin 2 and P_L [L] its accumulated value at time t:

$$Q_{Diff}(t) = S \times R_{Diff}(t) \text{ where}$$
$$R_{Diff}(t) = \begin{cases} 0 & \text{if} \quad P_L(t) < L \\ P_L(t) - L & \text{if} \quad 0 < P_L(t) - L < p_L(t) \\ p_L(t) & \text{if} \quad P_L(t) - L > p_L(t) \end{cases} \tag{11}$$

2.2.2.3. Recharge of the Aumelas-Thau Karst System

[30] Both diffuse (equation (11)) and allogenic (equation (9)) recharges are the input of an underground reservoir, for which two distinct outputs can be considered: one conveys GW outside from the Coulazou watershed, and mainly the Vène Spring during flood, and the other conveys groundwater toward the Coulazou River. Only this later output is considered in the model because it represents the GW contribution to surface flows in the river.

2.2.2.4. Karst GW Transfer to the River

[31] Outflow from the underground reservoir is controlled by 3 parameters: a Lag [T] parameter, a recession coefficient α [T^{-1}] and a drainage parameter D [L/T]. If the value of D is reached, the excess recharge is lagged (Lag) and the water level h [L] in the underground reservoir is linearly converted to discharge Q_{C*} in the riverbed. Thus, karst GW contribution to surface flows only occurs in the model when the combination of diffuse and allogenic recharge rates exceed D over the surface S of the reservoir. This GW contribution to surface flows is not distributed along the riverbed, but occurs in the model at a single point C* located in the middle of the karst riverbed (Figure 3), allowing comparison with measurements in the cave C (Figure 1).

[32] The linear relationship between water level and discharge reads

$$Q_{C*}(t) = S \times \alpha \times h(t - Lag) \tag{12}$$

The governing equation that gives the water level in the underground reservoir is solved explicitly using equation (13), where Δt is the time step (5 min). This water level is expressed in an arbitrary datum where $h > 0$ represents the activation of the upper drainage network:

$$h(t) = \max\left(0, h(t - \Delta t) + \Delta t \times \left[\frac{Q_{All}(t) + Q_{Diff}(t)}{S} - D - \alpha \times h(t)\right]\right) \tag{13}$$

where D represents the GW flow from the upper karst drainage network connected to the river toward the deeper compartment of the Aumelas-Thau karst system, and thus toward others karst outlets of the karst system, such as the Vène Spring (Figure 1) that are outside the Coulazou watershed. When $D = 0$, there is implicitly a no-flow boundary between the upper karst drainage network and the deeper compartment of the Aumelas-Thau karst system. This means that all the water that flows in the upper karst drainage network comes back downstream to the Coulazou River. This no flow boundary involves a GW divide between two hydrosystems, one being drained by the Coulazou River and the other by the outlets of the Aumelas-Thau karst system. This GW divide only occurs during high water table conditions in the karst aquifer when the discharge capacity of the Vène Spring is exceeded. Otherwise, D is expected to increase with the hydraulic gradient between the river and the karst aquifer, i.e., when h_W is low. The recession coefficient α determines the discharge in C^* for a given water level in the underground reservoir. Thus, at the basin scale, a low rate characterizes the drainage of an aquifer volume with great storage coefficient, i.e., a matrix volume or large karst voids poorly connected to the conduit system, while a high rate characterizes an efficient transfer system, i.e., the conduit system that only represents a small part (~1%) of the karst aquifer. Thus, the value of α as used in the model characterizes the GW flow regime, with conduit flow and matrix flow as end-members. The Lag parameter represents an additional GW transfer time within the underground reservoir because there is a lag associated with pressure transfer through not fully saturated karst conduits.

2.2.2.5. Simulated Discharge $Q_2(t)$ at the Basin Outlet (Q_2, Figure 1)

[33] The inflow that enters the river reach 2 is the sum of the simulated karst outflows Q_{C*}, the direct runoff on impervious area from the subbasin 2 and the simulated surface flows computed using equation (3) at the exit of the river reach 1 (Figure 3). This inflow is converted into surface flows at the exit of the river reach 2 using equation (3). The resulting discharge is added to the outflow from the subasin 3, which gives the simulated discharge $Q_2(t)$ in Q_2.

2.2.2.6. Initialization

[34] The river is not flowing before each flood event and the upper karst drainage network is inactive. Thus, there is no initial recession flow in the subbasin 1 and the initial

Table 2. Calibration Procedure According to the Initial Water Level Measured in W Prior to the Flood Event (h_W)

Water Table Condition Prior to the Flood	River Classification		Calibration Procedure		Number of Flood Events
	GW-SW Interactions	Flow Direction	Fixed Parameters	Number and List of Calibration Parameters	
Low, $h_W < 35$ m asl	Perched, mostly losing river, but eventually gaining in case of extreme rainfall event (e.g., 6 Sep 2005)	Losing	$\alpha = 0$ $L = \infty$ $D = \infty$ Lag = 100 min	(1), I	1
		Gaining	I = 7 m^3/s Lag = 100 min	(3) α, L, D	1
Medium to high, $35 < h_W < 47$ m asl	Perched or connected, losing or alternatively losing/gaining river, depending on recharge characteristics	Losing	$\alpha = 0$ $L = \infty$ $D = \infty$ Lag = 100 min	(1) I	1
		Losing/gaining	Lag = 100 min	(4) I, L, α, D	3
Very high, $h_W > 47$ m asl	Connected and gaining river		I = 0 D = 0 Lag = 100 min	(2) L, α	2

water level in the underground reservoir is set to 0, so that there is no karst outflow according to equation (12).

3. Results

3.1. Calibration

3.1.1. Outflows From Subbasin 1

[35] Calibration was carried out manually using the Nash coefficient [*Nash and Sutcliffe*, 1970] as a measure of goodness of fit between observed and simulated Q_1 (Figures 1 and 3). During calibration, best adjustments are obtained with *fc* set to 12 mm/h, which may be considered as an indirect measurement of the infiltration capacity of the soils derived from Oligocene detrital sedimentary rocks that are composed mainly of limestone pebbles embedded in a clayey matrix. However, this value has been modified to 5.2 mm/h and 7 mm/h for the two flood events occurring during the winter season (January 2006, see Table 1). The variation of *fc* over the hydrological cycle suggests that seasonal effects should be considered. The threshold flow for which base flow occurs (Q_0) has been successfully set to 0.8 m^3/s for each event. Nash coefficients vary between 75% and 95%, with an average value of 83% using all the data sets, which is relatively good since rainfall is considered in the model as uniform on the whole upstream catchment area (21 km^2 covered by only one rain gauge, Figure 1). Calibration of the hydrologic model on nonkarst terrains (subbasin 1) are not discussed in further detail since the purpose of this work is to focus on karst terrains; simulation results are, however, relatively good, which means that the chosen methods for runoff generation and transfer are suitable for reproducing flood dynamics in Q_1 at a 5 min time step. Some results are given in Figure 5 (left) as a comparison with results downstream from the karst aquifer (right).

3.1.2. Karst Terrains

[36] Results give Nash coefficients between 62% and 95% (see Table S2), with an average value of 86% using all the data sets. The Lag parameter has little influence on model calibration, as shown in section 3.2, and a fixed value of 100 min is used for each flood event. This value is in accordance with results from Gain and Phase spectrum analysis of Q_1 and Q_2 time series [*Bailly-Comte et al.*, 2008a], for which aligned discharge time series were used to remove the effect of the surface flow timing. The phase delay was interpreted as the delay of GW flows induced by underground runoff through nonsaturated karst conduits. As a result, the model requires at most 4 parameters for single event manual calibration: *I*, *L*, *D*, and α (Figure 3). These 4 parameters are fixed for a given flood, but are expected to vary from one flood event to another according to h_W.

[37] The calibration is done manually according to h_W and the classification of GW-SW interactions, as shown in Table 2; this means that an initial condition based on a prestorm water level in a well (h_W) is used to define the model structure, but not the values of the parameters: In the case of a losing river, only *I* needs to be calibrated in order to reproduce the hydrograph in Q_2. Thus, the infiltration capacity of the set of sinkholes in the riverbed, which is the maximum value of *I* can be determined in case of losing stream from a perched river. This occurred in October 2004 (Table 1 and Figure 5a). For this event, *I* is the only calibration parameter of the model, which allows the estimation of the infiltration capacity: $\max(I) = 7$ m^3/s. Then, in case of losing/gaining river or gaining river, *L*, α and *D* are adjusted to best fit observations in Q_2, while *I* is allowed to vary between 0 m^3/s and 7 m^3/s.

3.2. Postcalibration Sensitivity Analysis

[38] A simple postcalibration sensitivity analysis is carried out for the production and transfer methods on karst terrains by studying the behavior of the model to significant changes of $\pm 20\%$ in parameters made one at time, keeping all other parameter at their optimum values. This analysis has been done for L, D, α, Lag and n for the riverbed.

[39] For each parameter, only the mean of the relative variations resulting from the computation for each flood event is reported on Figure 4a. It shows for the 8 flood events the relative influence of each parameter change on the simulated flood peak, the total volume of the flood, the date of the flood peak and the Nash coefficient with respect to the corresponding value obtained with the optimum parameter set. This relatively basic sensitivity analysis clearly highlights that L, i.e., the initial losses that are supposed to be

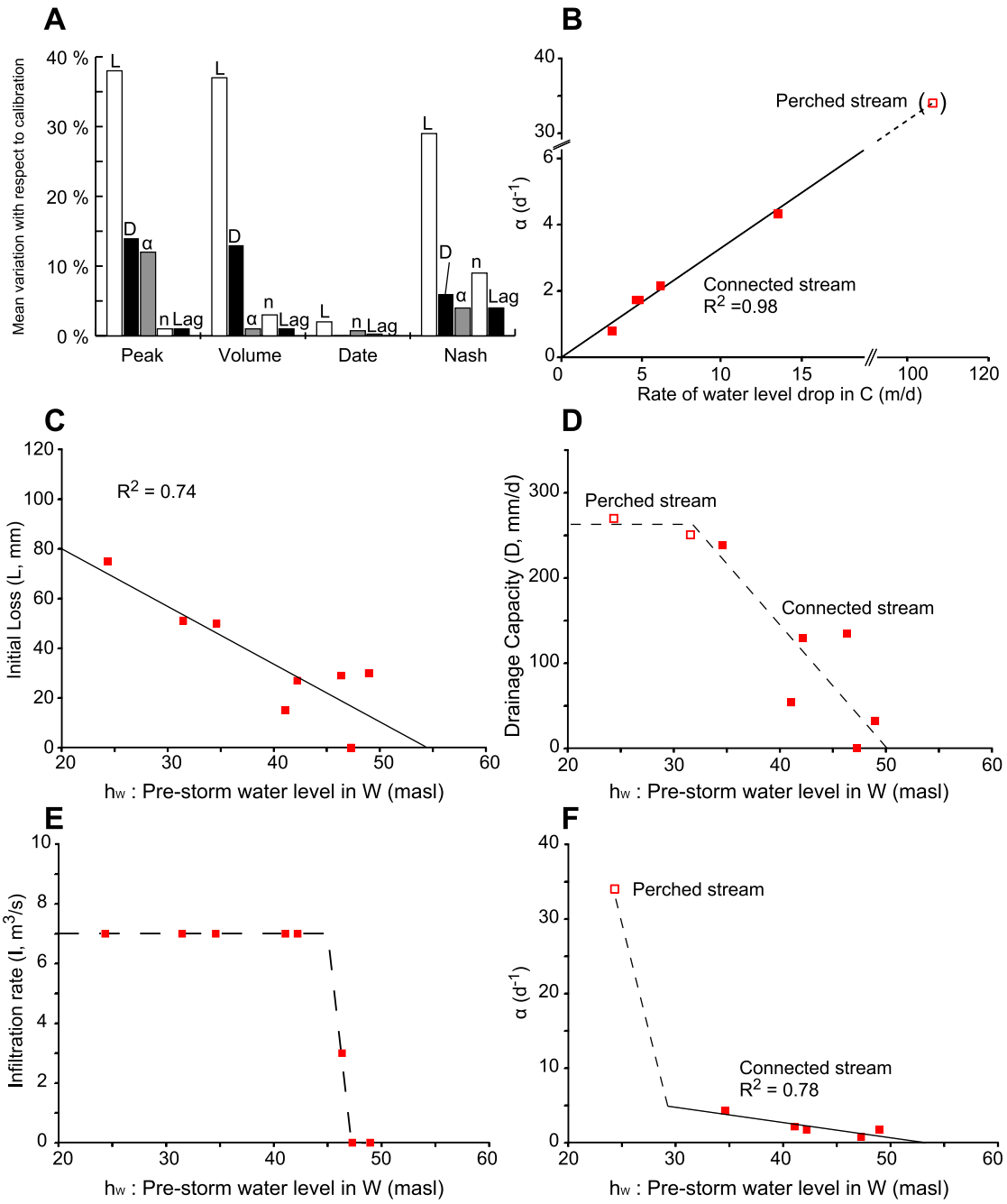

Figure 4. (a) Influence of a change of ±20% in each parameter on the simulation results expressed in percent of variation with respect to the optimum simulated value of the flood peak, the total volume of the flood, the date of the flood peak and the Nash coefficient. The y axis gives the mean result obtained from the 8 flood events. (b–f) Relationships between I, L, D and α and independent physical measurements in the aquifer; open and solid squares denote a case of perched or connected river, respectively. Solid lines are regression lines computed after calibration, while dashed lines are only used to suggest a trend in the data because no clear linear relationship exists.

related to the storage in epikarst and vadose zone, is the most sensitive parameter. This sensitivity is particularly strong on the peak simulation discharge, which is a relevant parameter when dealing with flash floods; however, the date when the flood peak occurs is not affected by these changes in parameters. It is also noticeable that variations of α, which are related to the volume of karst water drained toward the river (equation (12)), affect the simulated flood peak; this confirms that karst flow has a nonnegligible influence on the flood peak transfer.

4. Discussion

4.1. Comparison With Water Level Measurements in W and C

[40] Figure 4e shows a good and simple relationship between I and h_W. It shows that the infiltration capacity of

7 m^3/s for the set of sinkholes in the riverbed is reached for floods occurring during low water table conditions in the aquifer, whereas no infiltration occurs during high water table conditions. The change of behavior for h_W around 47 masl is consistent with previous considerations on the influence of the upper karst drainage system. Figure 4c shows that L is higher when h_W is low, which is consistent with a higher storage capacity of the vadose zone when it extends deeper. We also verify that D is close to 0 (Figure 4d) when h_W is high, and that D increases when h_W decreases, as discussed in section 2.2.2. The parameter α is determined only in the case of gaining (or alternatively losing and gaining) streams, which explains why results for only 6 flood events are shown in Figures 4b and 4f. The relationship between α and h_W (Figure 4f) shows at the basin scale that the storage coefficient of the drained material is higher (low α) for a higher h_W, which can be explained by the relative influence of the saturated matrix. In addition, it shows that the transfer is strongly different in the case of a gaining-perched river, when only conduit flow occurs (high α), than in the case of a gaining-connected river, illustrating the matrix restrained flow regime [*Bailly-Comte et al.*, 2010; *Kovács et al.*, 2005] when the hydraulic head in the carbonate matrix is higher than the one in the conduit system. In case of sinkhole backflooding along the Coulazou River, this matrix restrained flow regime can only occur for high water level condition prior to the flood.

[41] The water level in the upper karst drainage network can be measured in the cave C when it falls below the overflow level. For each flood, the water level time series shows a quasi linear decrease (i.e., water level evolution in cave C on Figure 5), allowing the estimation of the rate of the water level fall in the upper karst drainage network. The relationship between this measured decreasing rate and the fitted value of α in the model is given in Figure 4b, which shows a good linear relationship ($R^2 = 0.98$, the "Perched stream" point is not considered in this correlation analysis). This means that the fitted values of α are related to the hydrodynamics of the upper karst drainage network. According to equations 12 and 13, this linear relationship suggests a negligible drainage D toward the deeper part of the Aumelas-Thau karst system compared to sinkholes backflooding in the river when recharge stops, which is not the case if we convert the calibrated values of D in m^3/s. A possible explanation is that dh/dt as measured in the cave C is a local measure in the riverbed that is much more influenced by downstream sinkhole backflooding than by the drainage of the normally vadose zone toward the deeper part of the aquifer. In that case, it is consistent to see such a linear relationship, which is a direct consequence of the use of a first-order linear reservoir. In addition, it is consistent to find a low rate of water level drop for a low value of α, illustrating the matrix restrained flow regime of karst aquifer [*Bailly-Comte et al.*, 2010; *Kovács et al.*, 2005], and inversely in case of conduit flow regime. Accordingly, it is possible to assess the α coefficient as a function of the water table decreasing in the upper karst drainage network (measured in the field), when the latter is hydraulically connected to the Coulazou River.

4.2. Simulation in C* Compared to Measurements in C

[42] A direct comparison between measured water levels in C and simulated water levels in the reservoir (C* in Figure 3) requires the calibration of a datum and an equivalent efficient porosity, if such global parameters exist. As a result, hydrodynamics of GW in C is only compared to simulated karst outflows given by Q_{C*}. Figures 5a, 5b and 5c show the results for 3 flood events representative of a losing, alternatively losing/gaining or a gaining river, respectively.

[43] Figure 5a shows that the hydrograph in Q_2 is relatively well-reproduced if no karst outflows are simulated and only infiltration occurs through the sinkholes in the riverbed at a rate $I = 7$ m^3/s. This is consistent with measurements in C since the water table level increases but does not reach the overflow level; beside, the relatively high temperature in C characterizes SW storage in the cave.

[44] Figure 5b shows a more complex case for which water that initially fills the cave comes from the surface, characterized by a higher temperature at this time and a lower SpC. Then, the water table level in C reaches the overflow level; in addition, a mixing with waters of higher SpC and lower temperature highlights that the upper karst system drains the aquifer; at the same time, karst outflows are simulated in C*, with a strong influence on the resulting hydrograph in Q_2. As a comparison, runoff on nonkarst terrains explains the first little peak (Combe Escure, Figure 1) and the second little peak (transfer of the allogenic stream from Q_1), whereas the main peak is essentially due to a karst contribution to surface flows.

[45] Finally, Figure 5c shows how the karst aquifer influences the genesis and the transfer of the flood in the case of a gaining stream when no infiltration occurs in the riverbed ($I = 0$). The dynamics of simulated karst outflows are consistent with the water level measurements in C, as well as the temperature, which shows no mixing with SW that are around 5°C at this time.

[46] These results show the consistency of the hydrogeological concepts we used to simulate the genesis and the propagation of floods in such complex watersheds where karst hydrology drives the hydrologic response. We verify that two different processes can produce surface flows on this karst watershed: (1) the exceedance of the infiltration capacity of karst terrains, which only occurs in sinkholes that drain surface water, and especially in the riverbed that receives the allogenic water. This is "a localized Hortonian process" illustrated by $I < 7$ m^3/s in the model and (2) the exceedance of the drainage capacity D of the conduit network, inducing the increase of pressure head in conduits and ultimately producing sinkhole back flooding, and thus a karst contribution to surface flows from downstream to upstream at the basin scale. This is an adaptation of the concept of partial contributing area [*Dunne and Black*, 1970] to karst watersheds.

4.3. Influence of Karst on Flash Flood Genesis and Propagation

[47] Simulated times series of infiltrated waters through the riverbed and karst outflows in C* are used to assess the influence of the karst aquifer on both the flood peaks in the river and the cumulative volume at the exit of the aquifer. In the case of a losing river, the ratio $I/\max(Q_1)$ gives the negative influence of the karst aquifer on the peak transfer. In the case of an alternatively losing/gaining or a gaining river, the ratio $Q_{C*}(t_{\max})/Q_{C*}(t_{\max}) + Q_{Reach1}(t_{\max})$ gives the positive influence of the karst aquifer on the flood peak

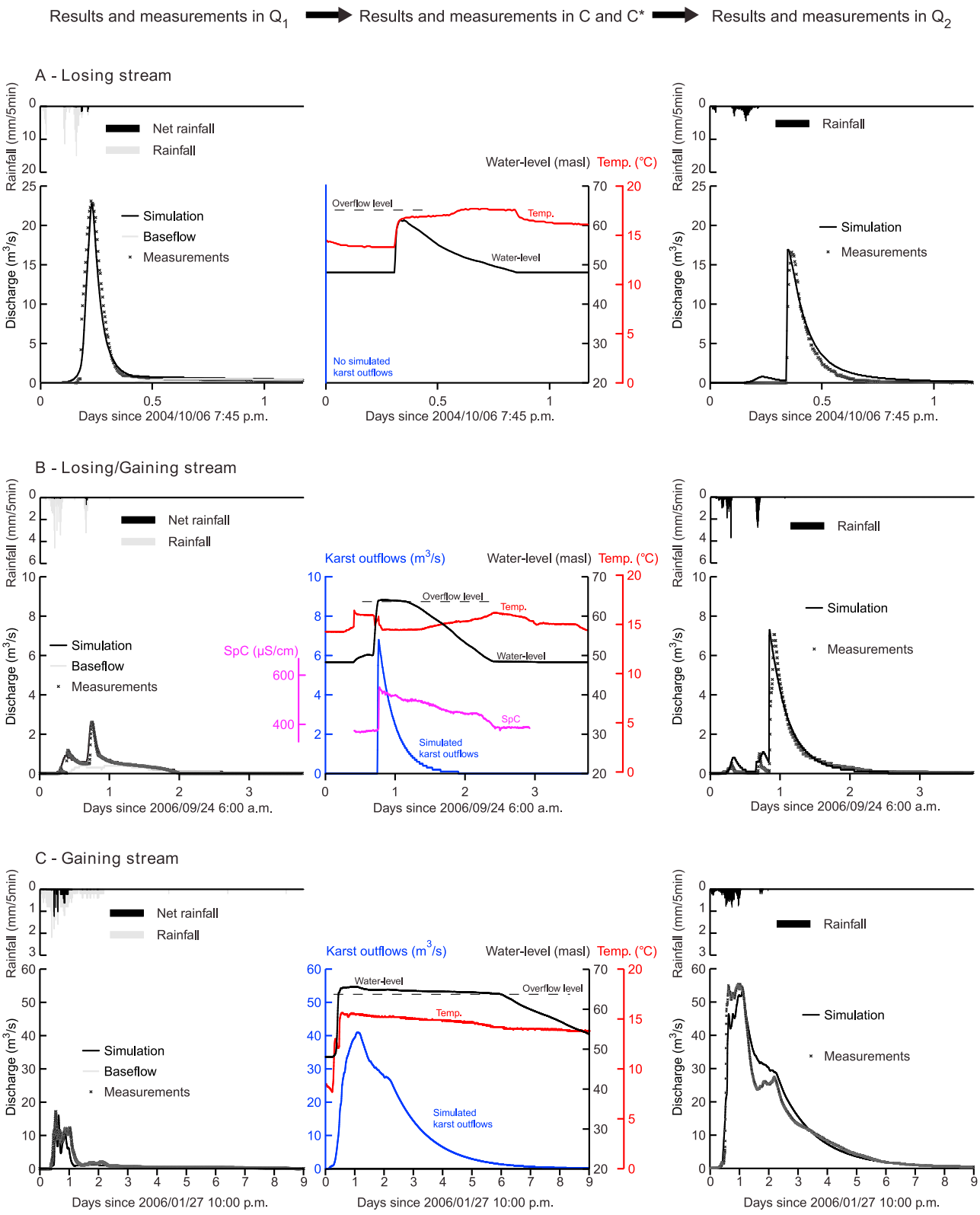

Figure 5. Some simulation results highlighting the karst contribution to surface flows for various types of hydrodynamic interactions between GW and SW: simulation and observation in (left) Q_1, (middle) C or C*, and (right) Q_2.

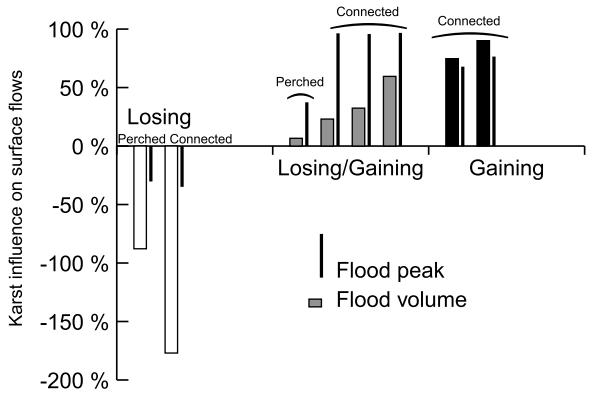

Figure 6. Karst influence on the flash flood peak and the cumulative runoff at the exit of the karst aquifer for various types of hydrodynamic connections and interactions between SW and GW using the 8 flood events recorded in the Coulazou River. See text for discussion for relevance of a losing or gaining stream for these computed karst influences on surface flows.

transfer, where t_{max} is the time when the estimated flow in C* is maximum and Q_{Reach1} is the simulated surface flows that joins C* (Figure 3). In terms of cumulated volumes, the karst influence is computed using the simulated water losses through the riverbed (negative influence) and the simulated karst outflows (positive influence), both normalized by the volume simulated in Q_2, which gives $\frac{\int Q_{C*} - \int Q_{Loss}}{\int Q_2}$.

[48] Figure 6 clearly shows that the influence of a karst aquifer on surface flood propagation can vary greatly for a same watershed. In the case of a losing river, it is noticeable that the karst does not strongly attenuate the flood peak compared to its attenuating effect on the flood volume, which reflects that the infiltration capacity of the karst riverbed is quickly reached during the flood transfer. At this site, Figure 6 illustrates that karst terrains have a relatively limited regulation effect on the flood peak propagation of flash floods, even if there are low water table conditions prior to the flood, as is typical in fall in the Mediterranean region. In the case of a connected losing/gaining river, the main part of the allogenic stream infiltrates until the increase of GW level induces surge flows in the river, which implies that the flood peak is a direct consequence of GW flows, as shown by the high contribution of karst GW to the flood peak (close to 100%, Figure 6). In the case of a gaining river, no infiltration of allogenic water occurs and the riverbed is fed by the aquifer as soon as the flood starts, which means that the flood peak at the exit of the karst aquifer is the sum of GW and surface flows. In that case, surface flow in the riverbed is driven by GW flow through the riverbed during the transfer of the whole flood event, which explains the high influence of karst on the flood volume. The only case of a flood for which the river has been identified as a perched losing/gaining river (Figure 6) shows a relatively little influence of the karst aquifer on the flash flood genesis and propagation, especially in terms of cumulative volumes. About 40% of the peak discharge is attributed to karst water because a part of the captured SW is added to fast infiltration and induces downstream a karst contribution to surface flows. However, these karst outflows only come from the drainage of karst conduits, which means that GW base flow is negligible (high α). As a result, in that case, the karst aquifer has a negligible effect on the flood volume in the river.

[49] Considering that the flood peak is the most important factor defining flash flood hazard, the regulation effect of the karst is limited for low water table conditions prior to the flood, while the aggravating effect may be higher than 80% for high water table conditions. Thus, GW contribution can be an aggravating factor in flash flood genesis on karst terrains, especially when the GW level prior to the flood is relatively close to the riverbed elevation. This shows that water table level monitoring might be a relevant factor for flash flood hazard assessment in karst areas, as suggested on other karst systems [*Roesch and Jourde*, 2006].

5. Conclusion

[50] A methodology combining time series analyses and flow modeling in both the Coulazou River and the karst aquifer allowed an assessment of the influence of karst on the genesis and propagation of flash flood using a conceptual semidistributed model with HEC-HMS 3.1. This work provides a first attempt at flash flood modeling in a karst watershed explicitly accounting for GW-SW interactions at a 5 min time step, which is the required time interval to describe such flood dynamics in karst systems. We show that it is reasonable to neglect the direct runoff on the karst terrains, which suggests that rainfall characteristics in space and time are only used to compute the diffuse recharge of the GW system; the cumulative height of precipitation which controls the GW recharge is thus the main characteristic of the rainfall event. Other characteristics (spatial distribution, duration, intensity etc.) are, however, crucial for assessing the surface flows on nonkarst terrains, since these surface flows recharge the karst aquifer, propagate over the karst terrains and may also induce a flash flood at the exit of the karst terrains, even in the case of a losing stream.

[51] This modeling approach is used as a tool for assessing SW-GW interactions during flood in the ephemeral karst stream. We define a model structure that is consistent with the hydrogeological concepts for this basin in order to physically interpret the parameters and especially the internal variable Q_{C*}, based on independent measurements in the karst aquifer. We show that the calibrated values for the 4 parameters I, L, D, and α of the underground reservoir and the resulting evolution of the internal variable Q_{C*} representing the karst contribution to surface flow can be compared to physical measurements in the karst/river system, while the simulated and measured discharge in Q_2 are in good agreement. It is shown how a classification of GW-SW interactions based on water table level in the karst aquifer prior to the flood can be used to define the number of calibration parameters for the underground reservoir model, which can reduce to one (I) in case of losing stream. The quality of the relationships between h_W and each parameter is however not sufficient for real-time model initialization, especially for L given the results of the post calibration sensitivity analysis for this parameter.

[52] The relationships between h_W and each parameter confirms that continuous water table level measurements in

W are a key element for understanding GW-SW hydrodynamic interactions in this karst watershed. As a perspective, based on Figures 4c–4f, another calibration procedure that explicitly uses h_W for the initialization of each parameter can be tested, which could lead to an original flood warning model using rainfall and water table level measurements in the aquifer as input. With this new objective, the model will require the use of a much larger data set, with calibration and validation done on separate events that covers all the different types of GW-SW interactions. Another way to improve the estimation of L (storage in the low-permeability portions of the epikarst and the vadose zone) would be to explicitly characterize the initial state of the vadose and epikarst zone. On the studied site, L is found to vary between 0 and 75 mm. Simple lumped models including conceptual evapotranspiration approaches at a monthly or a daily basis could be tested to better constrain the initialization of the L parameter. This would also require independent physical measurements of water fluxes in the vadose zone, and especially in the vadose conduits.

[53] Our results also give relevant information concerning the aggravating or regulating effect of karst terrains on flash floods. We show that the hydrodynamic response time of karst aquifers may be short enough to control the flood peak transfer in a river. Simulated time series of surface water losses and karst outflows have been used to quantify the karst contribution to surface flows. Conversely, the flood damping caused by GW recharge from SW appears to be relatively limited, even in very low water table condition prior to the flood event. Thus, our results demonstrate that karst watersheds may be considered as relatively poor systems of regulation but strong systems of amplification or generation of flash floods, depending on rainfall characteristics but also on GW level conditions prior to the flood, which means that the traditional emphasis on antecedent soil moisture for flash flooding is questionable for karst terrains.

[54] These results show that understanding GW-SW interactions is crucial for describing the flash flood dynamics in karst terrains. It also suggests that an efficient monitoring system for the forecasting and warning of karst flash floods should account for both water table level information within the aquifer and rainfall over the catchment area.

[55] **Acknowledgments.** The authors would like to thank Schlumberger Water Services for this productive collaboration and for the use of numerous data loggers within the framework of the MEDYCYSS observatory (Multi scale observatory of flood dynamics and hydrodynamics in karst, http://www.medycyss.org).

References

Arikan, A. (1988), MODALP: A deterministic rainfall-runoff model for large karstic areas/MODALP: Modèle déterministe pluie-débit pour les grands bassins karstiques, *Hydrol. Sci. J.*, *33*(4), 401–414, doi:10.1080/02626668809491262.

Bailly-Comte, V. (2008), Interactions hydrodynamiques entre les eaux de surface et les eaux souterraines en milieu karstique—Approche descriptive, analyse fonctionnelle et modélisation hydrologique appliquées au bassin versant expérimental du Coulazou, Causse d'Aumelas, France, PhD thesis, 223 pp., Univ. Montpellier 2, Montpellier, France. [Available at http://tel.archives-ouvertes.fr/tel-00319965/fr/.]

Bailly-Comte, V., H. Jourde, and S. Pistre (2008a), Transfer functions in a karst watershed using correlation and spectral analyses, case of the Coulazou watershed, Aumelas Thau system, south of France, paper presented at 13th IWRA World Water Congress, Int. Water Resour. Assoc., Montpellier, France.

Bailly-Comte, V., H. Jourde, A. Roesch, and S. Pistre (2008b), Mediterranean flash flood transfer through karstic area, *Environ. Geol.*, *54*(3), 605–614, doi:10.1007/s00254-007-0855-y.

Bailly-Comte, V., H. Jourde, A. Roesch, S. Pistre, and C. Batiot-Guilhe (2008c), Time series analyses for karst/river interactions assessment: Case of the Coulazou River (southern France), *J. Hydrol.*, *349*(1–2), 98–114, doi:10.1016/j.jhydrol.2007.10.028.

Bailly-Comte, V., H. Jourde, and S. Pistre (2009), Conceptualization and classification of groundwater-surface water hydrodynamic interactions in karst watersheds: Case of the karst watershed of the Coulazou River (southern France), *J. Hydrol.*, *376*(3–4), 456–462, doi:10.1016/j.jhydrol.2009.07.053.

Bailly-Comte, V., J. B. Martin, H. Jourde, E. J. Screaton, S. Pistre, and A. Langston (2010), Water exchange and pressure transfer between conduits and matrix and their influence on hydrodynamics of two karst aquifers with sinking streams, *J. Hydrol.*, *386*(1–4), 55–66, doi:10.1016/j.jhydrol.2010.03.005.

Bakalowicz, M. (2005), Karst groundwater: A challenge for new resources, *Hydrogeol. J.*, *13*(1), 148–160, doi:10.1007/s10040-004-0402-9.

Barrett, M. E., and R. J. Charbeneau (1997), A parsimonious model for simulating flow in a karst aquifer, *J. Hydrol.*, *196*(1–4), 47–65, doi:10.1016/S0022-1694(96)03339-2.

Bonacci, O. (2001), Analysis of the maximum discharge of karst springs, *Hydrogeol. J.*, *9*(4), 328–338, doi:10.1007/s100400100142.

Bonacci, O., I. Ljubenkov, and T. Roje-Bonacci (2006), Karst flash floods: An example from the Dinaric karst (Croatia), *Nat. Hazards Earth Syst. Sci.*, *6*, 195–203, doi:10.5194/nhess-6-195-2006.

Bonnet, A., and H. Paloc (1969), Les eaux des calcaires jurassiques du bassin de Montbazin-Gigean et de ses bordures (Pli de Montpellier et massif de la Gardiole, Hérault), *Bull. Bur. Rech. Geol. Min.*, *2*(3), 1–12.

Borga, M., P. Boscolo, F. Zanon, and M. Sangati (2007), Hydrometeorological analysis of the 29 August 2003 flash flood in the eastern Italian Alps, *J. Hydrometeorol.*, *8*(5), 1049–1067, doi:10.1175/JHM593.1.

Bouchaou, L., A. Mangin, and P. Chauve (2002), Turbidity mechanism of water from a karstic spring: Example of the Ain Asserdoune spring (Beni Mellal Atlas, Morocco), *J. Hydrol.*, *265*(1–4), 34–42, doi:10.1016/S0022-1694(02)00098-7.

Bourrier, R. (2001), Observations du fonctionnement du Coulazou aussi bien en surface que sous terre, report, Spéléoclub de Cournonterral, Cournonterral, France.

Camarasa Belmonte, A. M., and F. Segura Beltran (2001), Flood events in Mediterranean ephemeral streams (ramblas) in Valencia region, Spain, *Catena*, *45*(3), 229–249, doi:10.1016/S0341-8162(01)00146-1.

Delrieu, G., et al. (2005), The catastrophic flash-flood event of 8–9 September 2002 in the Gard Region, France: A first case study for the Cévennes-Vivarais Mediterranean Hydrometeorological Observatory, *J. Hydrometeorol.*, *6*(1), 34–52, doi:10.1175/JHM-400.1.

De Waele, J., M. L. V. Martina, L. Sanna, S. Cabras, and Q. A. Cossu (2010), Flash flood hydrology in karstic terrain: Flumineddu Canyon, central-east Sardinia, *Geomorphology*, *120*(3–4), 162–173, doi:10.1016/j.geomorph.2010.03.021.

Dörfliger, N., P. Fleury, and B. Ladouche (2009), Inverse modeling approach to allogenic karst system characterization, *Ground Water*, *47*(3), 414–426, doi:10.1111/j.1745-6584.2008.00517.x.

Doswell, C. A. (1994), Flash flood-producing convective storms: Current understanding and research, in *Report of the Proceedings (1994) of the U.S.-Spain Workshop on Natural Hazards (Barcelona, Spain, 8–11 June 1993)*, edited by J. Corominas and K. P. Georgakakos, pp. 97–107, Iowa Inst. of Hydraul. Res., Univ. of Iowa, Iowa City.

Doswell, C. A., H. E. Brooks, and R. A. Maddox (1996), Flash flood forecasting: An ingredients-based methodology, *Weather Forecast.*, *11*, 560–581, doi:10.1175/1520-0434(1996)011<0560:FFFAIB>2.0.CO;2.

Douchet, M. (2007), Puits de l'aven, Le Fil, *Bull. Liaison 17*, pp. 15–16, Comm. Natl. Plongée Souterraine, Marseille, France. [Available at http://souterraine.ffessm.fr/.]

Dreiss, S. J. (1983), Linear unit-response functions as indicators of recharge areas for large karst springs, *J. Hydrol.*, *61*(1–3), 31–44, doi:10.1016/0022-1694(83)90233-0.

Dunne, T., and R. D. Black (1970), Partial area contributing to storm runoff in a small New England watershed, *Water Resour. Res.*, *6*(5), 1296–1311, doi:10.1029/WR006i005p01296.

Fleury, P., V. Plagnes, and M. Bakalowicz (2007), Modelling of the functioning of karst aquifers with a reservoir model: Application to Fontaine de Vaucluse (south of France), *J. Hydrol.*, *345*(1–2), 38–49, doi:10.1016/j.jhydrol.2007.07.014.

Gaume, E., and C. Bouvier (2004), Analyse hydro-pluviometrique des crues du Gard et du Vidourle des 8 et 9 septembre 2002, *Houille Blanche*, *6*, 99–106, doi:10.1051/lhb:200406014.

Gaume, E., M. Livet, M. Desbordes, and J. P. Villeneuve (2004), Hydrological analysis of the river Aude, France, flash flood on 12 and 13 November 1999, *J. Hydrol.*, *286*(1–4), 135–154, doi:10.1016/j.jhydrol.2003.09.015.

Gaume, E., et al. (2009), A compilation of data on European flash floods, *J. Hydrol.*, *367*(1–2), 70–78, doi:10.1016/j.jhydrol.2008.12.028.

Hazan, R., and D. Lazarevitch (1967), Hydrologie en zone karstique au Maroc Sebou-Beth, in *Hydrologie des Roches Fissurées*, pp. 275–292, UNESCO, Paris. [Available at http://iahs.info/redbooks/a073/073030.pdf]

Huet, P., et al. (2003), Retour d'expérience des crues de Septembre 2002 dans le Sud Est, Minist. de l'Écol. et du Dév. Durable, Serv/ de l'Insp. Gén. de l'Environ., Paris. [Available at http://www.annales.org/re/2003/re32/huet63-72.pdf]

Jourde, H., A. Roesch, V. Guinot, and V. Bailly-Comte (2007), Dynamics and contribution of karst groundwater to surface flow during Mediterranean flood, *Environ. Geol.*, *51*(5), 725–730, doi:10.1007/s00254-006-0386-y.

Jukić, D., and V. Denić-Jukić (2004), A frequency domain approach to groundwater recharge estimation in karst, *J. Hydrol.*, *289*(1–4), 95–110, doi:10.1016/j.jhydrol.2003.11.005.

Jukić, D., and V. Denić-Jukić (2006), Nonlinear kernel functions for karst aquifers, *J. Hydrol.*, *328*(1–2), 360–374, doi:10.1016/j.jhydrol.2005.12.030.

Jukić, D., and V. Denić-Jukić (2009), Groundwater balance estimation in karst by using a conceptual rainfall-runoff model, *J. Hydrol.*, *373*(3–4), 302–315, doi:10.1016/j.jhydrol.2009.04.035.

Kovács, A., P. Perrochet, L. Király, and P.-Y. Jeannin (2005), A quantitative method for the characterisation of karst aquifers based on spring hydrograph analysis, *J. Hydrol.*, *303*(1–4), 152–164, doi:10.1016/j.jhydrol.2004.08.023.

Labat, D., R. Ababou, and A. Mangin (1999), Linear and nonlinear input/output models for karstic springflow and flood prediction at different time scales, *Stochastic Environ. Res. and Risk Assess.*, *13*, 337–364, doi:10.1007/s004770050055.

Labat, D., R. Ababou, and A. Mangin (2000a), Rainfall-runoff relations for karstic springs. Part I: Convolution and spectral analyses, *J. Hydrol.*, *238*(3–4), 123–148, doi:10.1016/S0022-1694(00)00321-8.

Labat, D., R. Ababou, and A. Mangin (2000b), Rainfall-runoff relations for karstic springs. Part II: Continuous wavelet and discrete orthogonal multiresolution analyses, *J. Hydrol.*, *238*(3–4), 149–178, doi:10.1016/S0022-1694(00)00322-X.

Larocque, M., A. Mangin, M. Razack, and O. Banton (1998), Contribution of correlation and spectral analyses to the regional study of a large karst aquifer (Charente, France), *J. Hydrol.*, *205*(3–4), 217–231, doi:10.1016/S0022-1694(97)00155-8.

Le Moine, N., V. Andréassian, and T. Mathevet (2008), Confronting surface- and groundwater balances on the La Rochefoucauld-Touvre karstic system (Charente, France), *Water Resour. Res.*, *44*, W03403, doi:10.1029/2007WR005984.

Llasat, M. C., et al. (2010), High-impact floods and flash floods in Mediterranean countries: The FLASH preliminary database, *Adv. Geosci.*, *23*, 47–55, doi:10.5194/adgeo-23-47-2010.

Long, A. J. (2009), Hydrograph separation for karst watersheds using a two-domain rainfall-discharge model, *J. Hydrol.*, *364*(3–4), 249–256, doi:10.1016/j.jhydrol.2008.11.001.

Long, A. J., and R. G. Derickson (1999), Linear systems analysis in a karst aquifer, *J. Hydrol.*, *219*(3–4), 206–217, doi:10.1016/S0022-1694(99)00058-X.

López-Chicano, M., M. L. Calvache, W. Martín-Rosales, and J. Gisbert (2002), Conditioning factors in flooding of karstic poljes—The case of the Zafarraya polje (south Spain), *Catena*, *49*(4), 331–352, doi:10.1016/S0341-8162(02)00053-X.

Mangin, A. (1984), Pour une meilleure connaissance des systemes hydrologiques a partir des analyses correlatoire et spectrale, *J. Hydrol.*, *67*(1–4), 25–43, doi:10.1016/0022-1694(84)90230-0.

Maréchal, J. C., B. Ladouche, and N. Dörfliger (2008), Karst flash flooding in a Mediterranean karst, the example of Fontaine de Nîmes, *Eng. Geol.*, *99*(3–4), 138–146, doi:10.1016/j.enggeo.2007.11.013.

Mijatovic, B. (1988), Catastrophic flood in the polje of Cetinje in February 1986, a typical example of the environmental impact of Karst, *Environ. Geol.*, *12*(2), 117–121.

Nash, J. E., and J. V. Sutcliffe (1970), River flow forecasting through conceptual models part I—A discussion of principles, *J. Hydrol.*, *10*(3), 282–290, doi:10.1016/0022-1694(70)90255-6.

Norbiato, D., M. Borga, S. Degli Esposti, E. Gaume, and S. Anquetin (2008), Flash flood warning based on rainfall thresholds and soil moisture conditions: An assessment for gauged and ungauged basins, *J. Hydrol.*, *362*(3–4), 274–290, doi:10.1016/j.jhydrol.2008.08.023.

Norbiato, D., M. Borga, R. Merz, G. Blöschl, and A. Carton (2009), Controls on event runoff coefficients in the eastern Italian Alps, *J. Hydrol.*, *375*(3–4), 312–325, doi:10.1016/j.jhydrol.2009.06.044.

Padilla, A., and A. Pulido-Bosch (1995), Study of hydrographs of karstic aquifers by means of correlation and cross-spectral analysis, *J. Hydrol.*, *168*(1–4), 73–89, doi:10.1016/0022-1694(94)02648-U.

Padilla, A., and A. Pulido-Bosch (2008), Simple procedure to simulate karstic aquifers, *Hydrol. Processes*, *22*(12), 1876–1884, doi:10.1002/hyp.6772.

Panagopoulos, G., and N. Lambrakis (2006), The contribution of time series analysis to the study of the hydrodynamic characteristics of the karst systems: Application on two typical karst aquifers of Greece (Trifilia, Almyros Crete), *J. Hydrol.*, *329*(3–4), 368–376, doi:10.1016/j.jhydrol.2006.02.023.

Rahnemaei, M., M. Zare, A. R. Nematollahi, and H. Sedghi (2005), Application of spectral analysis of daily water level and spring discharge hydrographs data for comparing physical characteristics of karstic aquifers, *J. Hydrol.*, *311*(1–4), 106–116, doi:10.1016/j.jhydrol.2005.01.011.

Rimmer, A., and Y. Salingar (2006), Modelling precipitation-streamflow processes in karst basin: The case of the Jordan River sources, Israel, *J. Hydrol.*, *331*(3–4), 524–542, doi:10.1016/j.jhydrol.2006.06.003.

Roesch, A., and H. Jourde (2006), Incidence d'une gestion active de la ressource en eau en milieu karstique sur le risque hydrologique. Exemple du Fleuve Lez (Montpellier, France), paper presented at 2nd Congrès International Gestion Intégrée des Ressources en Eaux et Défis du Développement Durable (GIRE3D), Assoc. Int. des Hydrogéol., Marrakesh, Morocco.

U.S. Army Corps of Engineers (USACE) (2002a), HEC-HMS (Hydrologic Engineering Center-Hydrologic Modeling System), applications guide, CPD-74*C*, 117 pp., Hydrol. Eng. Cent., Davis, Calif.

U.S. Army Corps of Engineers (USACE) (2002b), HEC-RAS, river analysis system, v3.1 (CPD-68), Hydrol. Eng. Cent., Davis, Calif.

Virginia Department of Conservation and Recreation (2006), Hydrologic modeling and design in karst, *Tech. Bull. 2*, 13 pp., Stormwater Manage. Program, Richman, Va.